https://doi.org/10.46813/2024-150-020

HARDENING BEHAVIOR OF ADVANCED STRUCTURAL ALLOYS UNDER ION IRRADIATION

G.D. Tolstolutska, M.A. Tikhonovsky, S.O. Karpov, V.K. Karpach
National Science Center "Kharkov Institute of Physics and Technology", Kharkiv, Ukraine
E-mail: karpofff@kipt.kharkov.ua

In this study, a series of recently developed alloys, including multi-principal element alloys with FCC and BCC phase structure, ODS-modified austenitic steel, and T91 ferritic-martensitic steel modified with severe plastic deformation have been investigated with respect to the hardening/embrittlement phenomenon under irradiation. Samples of all materials were irradiated under identical conditions with 1.4 MeV Ar ions at room temperature. Transmission electron microscopy (TEM) was used to characterize the radiation defects and microstructural changes. Nanoindentation was employed to measure the effect of ion irradiation on hardening. The dependence of the hardening parameters on the irradiation dose, their relationship with the evolution of the microstructure was studied. It was found, that the developed alloys exhibited a reduced susceptibility to irradiation induced hardening compared to that of conventional SS316 and 18Cr10NiTi stainless steels. The study discusses the mechanisms that can affect the radiation hardening behavior in examined materials.

PACS: 61.80.-X, 81.40.CD

INTRODUCTION

Advances in nuclear technology have led to the development of next-generation reactors that are safer, more reliable and more cost-effective. The deployment of these advanced reactors depends on the development of new radiation-resistant materials, as the integrity of the structural materials within nuclear reactors is critical to the overall safety of the power station. A comprehensive understanding of the effects of irradiation on the mechanical properties of these potential materials is essential for their further development.

Irradiation of structural materials at reactor-relevant temperatures can lead to significant changes in microstructure, mechanical properties, and even external dimensions of structural components. This phenomenon, initiated at the nanoscale with the formation and interaction of point defects, escalates to macroscopic effects such as swelling, anisotropic growth, radiation creep, and phase transformations, which are critical for reactor safety [1]. The co-evolution of microstructural components plays a key role in these radiation-induced phenomena. Furthermore, irradiation can promote the formation and growth of various microstructural defects such as solute clusters, dislocation loops, and nanovoids.

These defects impede dislocation glide, leading to hardening and potentially detrimental embrittlement. It is crucial to note that hardening and embrittlement are interconnected, implying that a quantitative understanding of hardening is essential for assessing the integrity of reactor structural components [2]. The degree of irradiation-induced hardening and embrittlement is determined by a complex interplay of metallurgical and irradiation factors, underscoring the importance of understanding these mechanisms for the safety of nuclear power systems.

The investigation of radiation-induced hardening in structural alloys of reactors has garnered significant interest, with comprehensive studies conducted over recent decades from both practical and theoretical perspectives [3]. This phenomenon is associated with the formation of nanometric defects, encompassing clusters and precipitates of solute elements, grain-boundary segregation, and matrix defects such as vacancies, interstitials, and their aggregation into dislocation loops. These microstructural obstacles act as barriers to dislocation motion, thereby reducing material ductility while increasing yield strength.

A thorough and consistent characterization of these obstacle families is essential for each material within the study. Consequently, it is advisable to combine these observations into a unified scheme to determine to what extent the identified nanoscale microstructural features can explain the quantitative hardness increase caused by irradiation.

In this study, a series of recently synthesized/ modified alloys, including multi-principal element alloys with FCC and BCC phase structure, ODS-modified 18Cr10NiTi austenitic steel, T91 ferritic-martensitic steel modified with severe plastic deformation have been investigated in relation to the hardening/embrittlement phenomenon under irradiation. The dependence of the hardening parameters on the irradiation dose, their relationship with the evolution of the microstructure is studied. Comparison of the obtained data with data for conventional stainless steels after irradiation under identical conditions was carried out.

1. MATERIALS AND METHODS

A number of materials have been examined in this study in relation to radiation induced hardening. These included / specifically

The new lightweight multi-principal element (MPEA) titanium-based alloy 61Ti10Cr7Al11V11Nb (at. %) (calculated density 4.95…5.59 g/cm^3) with non-equal molar ratio, hereinafter referred to as Ti-MPEA, was obtained by arc melting using a non-consumable tungsten electrode in a pure argon atmosphere. The purity of the initial components was not less than 99.9%. To equalize the chemical composition, the cast alloys were homogenized at a temperature of 900 °C for

15 min in pure argon, followed by quenching in air. More details on the methods of alloy production and the examination of its structure and properties are given in [4, 5].

Non-cobalt 20Cr40Fe20Mn20Ni (mass.%) high entropy alloy (hereinafter referred to as HEA) was produced by arc melting in a water-cooled copper mould filled with high-purity argon. The purity of the alloying elements was above 99.9%. Alloys were subjected to thermomechanical treatment (TMT) that consisted of deformation by rolling at room temperature from 6 to 0.5 mm. Finishing annealing of 0.5 mm specimens was carried out at 850 °C for 1 h.

The mechanical alloying of HEA powders with oxides and receiving 20Cr40Fe20Mn20Ni-ODS powders (hereinafter referred to as HEA-ODS) was carried out in a ball mill in an inert atmosphere of argon [6]. 15 g of alloy powder with a dispersion of ≤ 300 μm was placed into a steel container of a high-energy planetary ball mill and 0.5% (mass) a pre-synthesized powder of composition $80\%Y_2O_3 + 20\%ZrO_2$ (in mol.%) with a dispersion of about 14 nm was added. The synthesized powder was compacted by cold pressing, followed by sintering in vacuum at a temperature of 1100 °C for 30 min. Then, the billets were rolled into a 0.5 mm thick strip with intermediate annealing at 850 °C. At the final stage, the strip was annealed at 1100 °C for 1 h.

The ODS-modified 18Cr10NiTi austenitic steel (hereinafter referred to as 18Cr-ODS) was produced by mechanical alloying of steel powder with 0.5 wt.% of $80\%Y_2O_3$ - $20\%ZrO_2$ nano-oxides followed by compacting and thermo-mechanical treatment. A detailed technological procedure of production is described in [7].

T91 ferritic-martensitic steel of composition 9Cr-1Mo with minor alloying elements of Ni, Nb, V, and C was delivered as hot rolled and heat-treated plates with a thickness of 40 mm. The heat treatment consisted of a normalization treatment at 1040 °C for 30 min followed by air cooling and then tempered at 730 °C for 60 min followed by air cooling to room temperature. The microstructure of as-received T91 steel (hereinafter sample code T91-M) represents the tempered martensite structure with the occurrence of boundaries of former austenite grains and subgrains.

An applying of SPD by the "upsetting-extrusion" method led to an effective decrease of the average grain size from 8 μm in the as-received state to 100 nm after SPD. After heat treatment at 600 °C for 25 h (hereinafter, sample code T91-MSPD), sufficiently large grains of typical "ferritic" morphology have formed. "Broken" martensite in some zones is transformed into a more "classic" [8].

Two solution annealed commercial type AISI316 (sample code SS316) and 18Cr10NiTi (sample code 18Cr) stainless steels with typical compositions have been used in the current study as reference materials. Samples for irradiation and subsequent studies were made from the obtained ingots using wire-cut electrical discharge machining.

Samples of all materials were irradiated with 1.4 MeV argon ions at room temperature (RT) in a dose range of 0.1…10 dpa. These mid-range doses are evaluated at a depth of ~ 0.25 μm. All irradiations were carried out with the accelerating-measuring system 'ESU-2' [9], which contain Van de Graaf accelerator. The depth distribution of Ar atoms concentration and damage was calculated by SRIM 2008 and shown in Fig. 1. The damage calculations are based on the Kinchin-Pease model, with a displacement energy for each alloying element was set to 40 eV, as recommended in ASTM E521-96 (2009) [9].

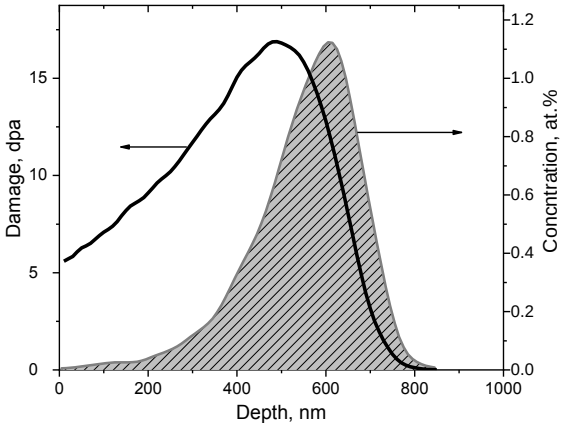

Fig. 1. Calculated depth distribution of damage and concentration of 1.4 MeV Ar^+ ions in 18Cr10NiTi steel

Nano-hardness measurements were carried out by Nanoindenter G200 with a Berkovich type indentation tip. Prior to ion irradiation surfaces of the samples were mechanically polished initially with sandpapers of varying grits and finally electrolytically polished using 95% methanol and 5% perchloric acid solution at a temperature of -20 °C with an applied voltage of 30 V to remove mechanically damaged layer. Each sample was applied at least 20 points at a distance of 35 μm from each other. A maximum indenter displacement of 1 μm was used for all measurements. The Oliver-Pharr method was used for determination of the hardness [10].

Transmission electron microscopy (TEM) investigations were performed using JEM-100CX and JEM-2100 microscopes. Details of the specimens thinning for TEM examination have been presented elsewhere [4]. Standard bright-field technique was used to characterize the irradiation-induced microstructural changes.

2. RESULTS AND DISCUSSION

In the present study, the nano-hardness as a function of the indenter displacement for unirradiated and irradiated materials has been measured. By processing the hardness profiles using the Nix-Gao approach [10], the bulk-equivalent hardness H_0 has been evaluated.

Fig. 2 shows the nano-hardness H_0^{unirr} of all studied materials prior to ion irradiation. Obviously, BCC alloys exhibit higher hardness values in unirradiated state compared to those in FCC alloys.

The hardness of unirradiated FCC-structured SS316 and 18Cr10NiTi austenitic steels are almost the same. Meanwhile, the initial nano-hardness of 18Cr-ODS steel was found to be ~ 1.5 times higher. Fig. 3 illustrates the microstructures observed in these steels, featuring defects across multiple scales. The identified microstructural characteristics appear to influence the primary hardness mechanisms within the materials.

The microstructure of AISI 316 (see Fig. 3,a) after solution annealing consists of polyhedral austenitic grains with twinning typical for FCC microstructure. The average austenitic grain size in this state is about (35±5) μm. Additionally, a small amount of δ-ferrite was recorded. No precipitates were observed at the grain boundaries (GB) of solution annealed steels.

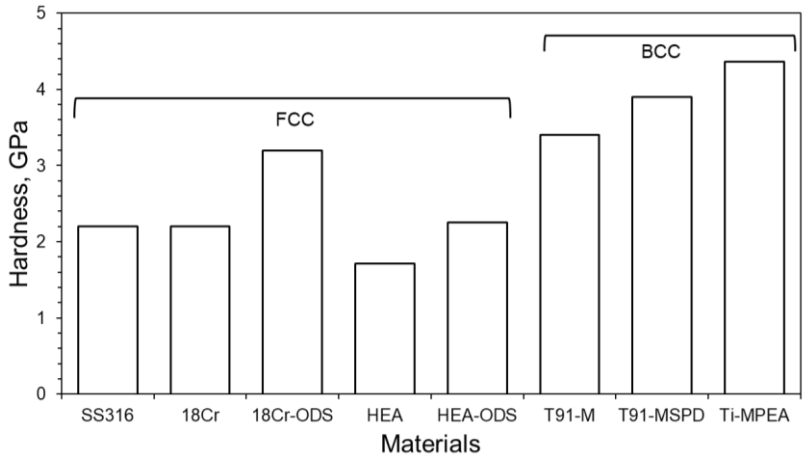

Fig. 2. Nano-hardness of unirradiated FCC- and BCC-structured materials

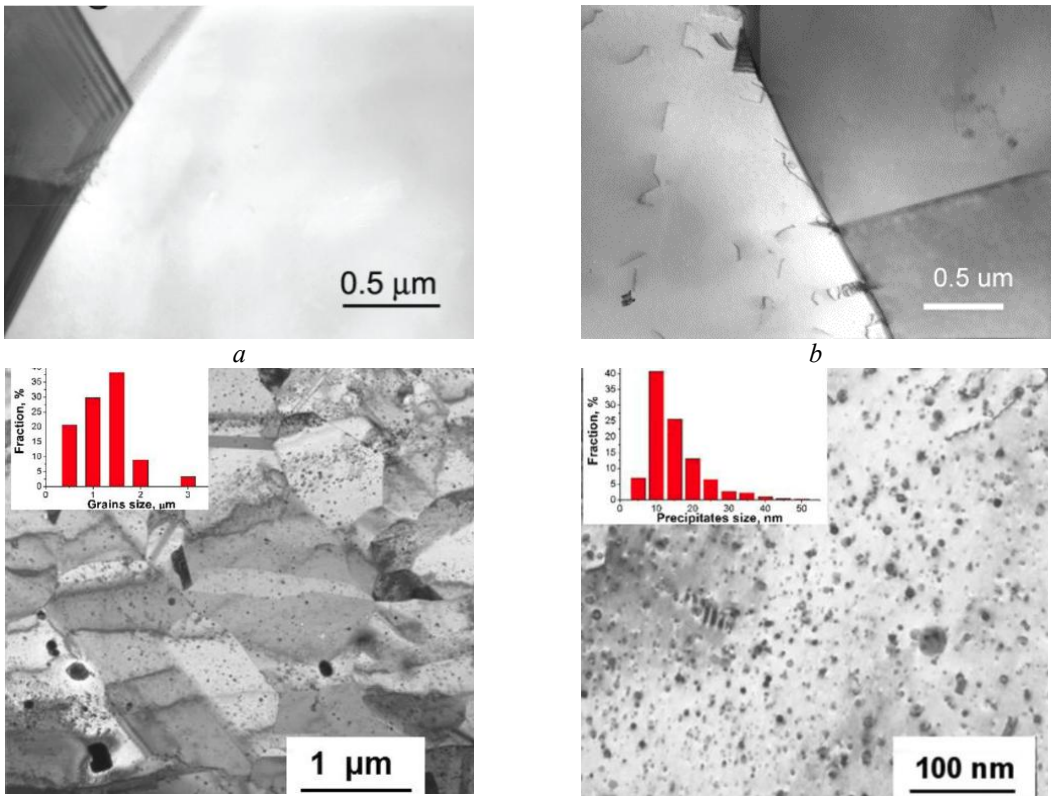

a *b* *c* *d*

Fig. 3. Typical TEM micrographs of pre-irradiation microstructure of SS316 (a), 18Cr10NiTi(b), and 18Cr10NiTi-ODS steels (c, d) [7]

18Cr10NiTi steel was observed to be two-phase after solution annealing (see Fig. 3,b). The majority were austenite grains (size ~ 30 μm), but small crystallites of δ-ferrite were also observed at a volume fraction of 2…3%. Annealing twins, precipitates of second phase (carbides and titanium carbonitrides) and dislocations (~ 10^8 cm^{-2}) were seen in austenitic grains. Many of perfect dislocation were observed to exhibit partial dislocation separation with stacking fault formation.

The microstructure of 18Cr-ODS steel is characterized by fine grains with an average size of ~ 1.2 μm (see Fig. 3,c). High-density oxide nano-precipitates with near-uniform distribution were observed within the matrix of each grain (see Fig. 3,d). Precipitate size varies from several nanometers to hundreds of nanometers, but the larger sizes are several orders less in density, and thus their contribution to both concentration and average size is negligible. The average size of nano-precipitates is estimated at ~ 10 nm and their average density is ~ $7.3 \cdot 10^{21}$ m^{-3}. Electron microprobe analysis of the ODS-steel indicated the presence of Y, Zr, Ti, and O in these precipitates. A more detailed study using electron diffraction showed

that these precipitates are complex oxides with pyrochlore structure $Y_2(Zr,Ti)_2O_7$ [7].

Microstructural features revealed by transmission electron microscopy are responsible for the observed differences in hardness. Particularly, a microstructure characterized by finer grains typically leads to enhanced strength and superior toughness compared to an identical alloy with larger grains. Moreover, the presence of dispersed ultrafine particles impedes dislocation motion and serves as a factor for precipitation strengthening. Therefore, the rise in hardness observed in the 18Cr-ODS steel is likely attributable to the combined effects of grain size reduction and oxide nano-precipitates.

In this study, it was observed that among the materials investigated, the FCC HEA exhibited the lowest hardness in initial state (see Fig. 2). The addition of yttrium and zirconium oxides for strengthening purposes did not substantially enhance the hardness. Fig. 4 shows the microstructure of both HEA and its strengthened version.

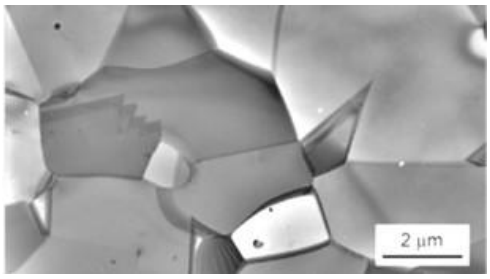

a

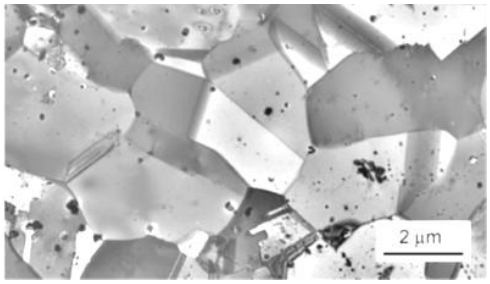

b

Fig. 4. Typical TEM micrograph of 20Cr-40Fe-20Mn-20Ni (a), ODS-20Cr-40Fe-20Mn-20Ni (b) high-entropy alloys [6]

XRD analysis revealed that both the as-cast and thermomechanically treated alloys, following a final heat treatment at 1100 °C, consisted of a single-phase FCC-crystal lattice. The average grain sizes of the HEA and ODS-HEA were determined to be 3.47 and 1.61 μm, respectively, which are not significantly different. The initial dislocation densities in the examined alloys varied within the range of $(1.7…2.5)\cdot10^{12}$ m^{-2}.

Generally, the microstructures observed in HEAs may include precipitates at a variety of scales, twinning, strain-induced martensite, and recrystallization. These microstructural features determine the primary strengthening mechanisms, which involve precipitation hardening, TWIP, martensite formation, and dynamic recrystallization [11]. The slight increase in hardness observed in HEA-ODS compared to ordinary HEA (see Fig. 2) can be attributed to the existence of dispersed ultrafine oxide nano-precipitates.

The initial nano-hardness values are markedly increased in steels and alloys that crystallize as body-centered cubic (BCC) structures. In this case, the nanohardness is approximately 1.8–2.2 times higher compared to the reference stainless steels (see Fig. 2).

The microstructure of as-received T91-M steel represents the tempered martensite structure with the occurrence of boundaries of former austenite grains and subgrains (Fig. 5,a). These boundaries are decorated with precipitates of $M_{23}C_6$ carbides. The average size of the former austenite grains is ~ 20 μm, and the average size of subgrains is ≈ 8 μm. Martensite lamellas with a transverse size of 0.25…0.5 μm are observed inside the former austenite grains. In additions, a significant number of small precipitates of ≤ 50 nm in size, which are usually referred to as MX-type phases is also observed [8].

The microstructure of T91-MSPD steel after applying of SPD by the "upsetting-extrusion" method comprises a broken martensite type structure and grains with the average size 100 nm. After heat treatment at 600 °C for 25 h, sufficiently large grains of typical "ferritic" morphology have formed (see Fig. 5,b), which appear to be the result of recrystallization of fine grains of former austenite or fine-grained areas of "broken" martensite. "Broken" martensite in some zones is transformed into a more "classic" one as a result of the enlargement of martensite lamellas with the average grain size increasing up to 210 nm. The average size and density of $M_{23}C_6$ precipitates is 120 nm, and $4.2\cdot10^{19}$ m^{-3}, respectively. Carbides of the MX type having the size of ≤ 24 nm and density of $2.6\cdot10^{20}$ m^{-3} are more evenly distributed in the grains.

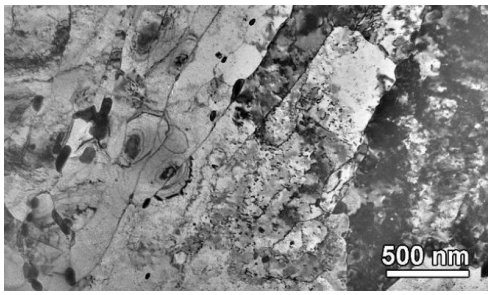

a

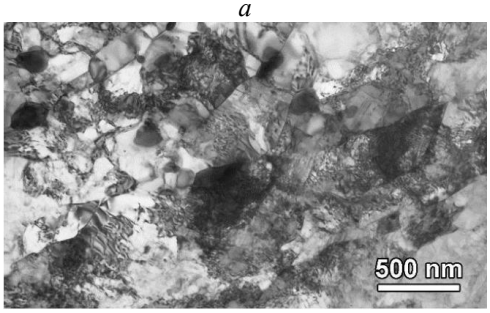

b

Fig. 5. Microstructure of as-received T91-M (a) and T91-MSPD (b) steels [8]

Most of the strengthening methods used in conventional alloys include solid solution strengthening, grain refinement strengthening, dual phase strengthening, phase strengthening, and precipitation

strengthening [12]. All of these mechanisms operate to some extent in BCC steels, resulting in their high initial hardness.

The initial microstructure of a Ti-MPEA alloy before irradiation is shown in Fig. 6. XRD analysis of the alloy revealed that Ti-MPEA has a single BCC structure without a second phase. As a result of annealing at 900 ºC for 15 min, the average grain size in the 61Ti10Cr7Al11V11Nb alloy was 68 μm. Within the scope of this study, Ti-MPEA alloy exhibited exceptionally high intrinsic hardness even prior to irradiation despite the coarse grain size and no obvious availability nanoprecipitates (see Fig. 2). The reason for high hardness may be solid-solution hardening – the attainment of an increase in matrix strength through addition of different soluble elements. The distortion of atomic lattice caused by the misfit of atomic radius inhibits dislocation movement [12].

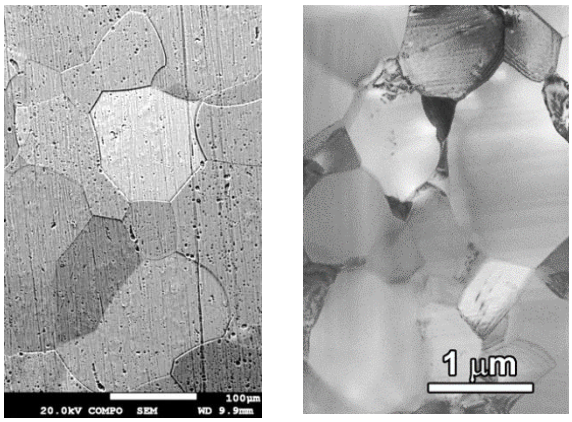

a *b*

Fig. 6. SEM (a) and TEM (b) micrographs for microstructure of 61Ti10Cr7Al11V11Nb alloy after annealing at 900 °C for 15 min

In this study, the samples of aforementioned materials were irradiated under an identical condition with 1.4 MeV Ar ions at room temperature. Generally, radiation strengthening is highly dose-dependent at low fluences and tends to saturation at doses exceeding some critical value. As an example, Fig. 7 illustrates the dose dependences of bulk-equivalent hardness for irradiated HEA, ODS-HEA, and SS316.

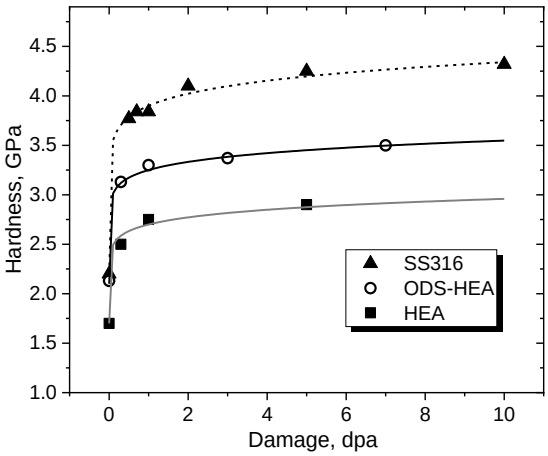

Fig. 7. The dose dependence of hardness of ion-irradiated HEA, ODS-HEA, and SS316 [6]

As evident from Fig. 7, the most significant effect of irradiation occurs at a dose of approximately 1 dpa, with a gradual transition towards a quasi-saturation mode at higher fluences. Notably, G.S. Was et al., in their analysis of radiation-induced hardening data for identical heats of proton- and neutron-irradiated 304SS and 316SS, have demonstrated that the radiation hardening of austenitic steels saturates after a few dpa [13]. A similar tendency has been observed in steels and alloys that are in the focus of current study. Specifically, radiation hardening of BCC alloys also tends to saturation at about a few dpa. However, the magnitude of the hardening is almost half compared to austenitic alloys. The initial hardness and the radiation hardening, denoted as $\Delta H = H_0^{irr} - H_0^{unirr}$ are shown in Fig. 8. Hardness values H_0^{irr} for irradiated materials were taken at dose of 10 dpa.

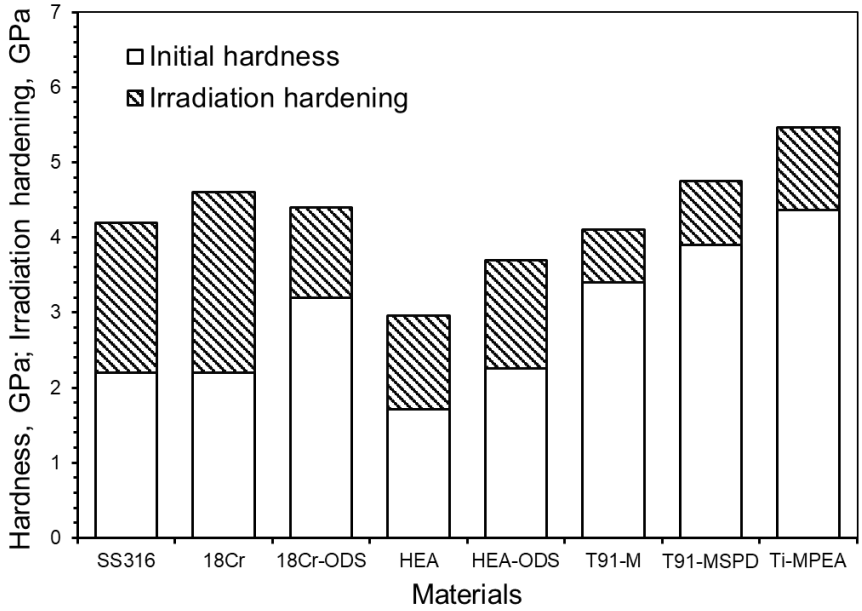

Fig. 8. The initial hardness and the radiation hardening for the studied materials irradiated under identical conditions

Conventional SS316 and 18Cr10NiTi steels exhibited the highest levels of irradiation hardening, while other alloys examined in this study showed lower susceptibility to this phenomenon. Radiation-induced hardening in metals is generally associated with the formation of dislocation loops which greatly impede the movement of dislocations. In the case of Ar-ion irradiation, an additional hardening effect can be attributed to the radiation-induced cavity formation [7, 14]. TEM analysis of Ar-irradiated specimens revealed significant differences in the irradiation-induced microstructure between the near-surface layer and deeper areas of the material. For instance, Fig. 9 shows the microstructure of Ar-irradiated 18Cr steel. Within the first 400 nm from the irradiated surface, a predominantly "black dots" and dislocation loops were observed (see Fig. 9, a). In addition, nano-scale cavities were found at depths ranging from 500 to 700 nm (see Fig. 9, b). These findings are consistent with the calculated deposition of argon (see Fig. 1), as Ar concentration in this deeper layer reaches ~ 1 at.%. The cavities, with an approximate size of 1 nm, showed a near-spherical shape, indicating that the cavities formed under the current irradiation conditions are likely to be Ar-filled bubbles.

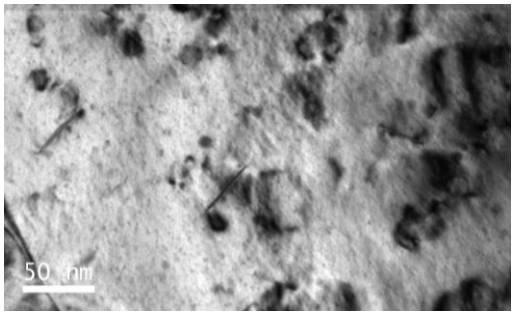

a

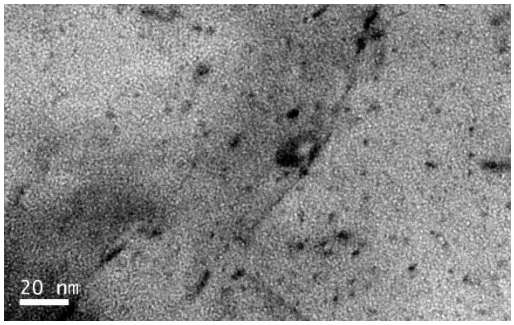

b

Fig. 9. Microstructure of 18Cr10NiTi steel after Ar^+ irradiation at T_{room} at a depth of 100 nm (a) and 600 nm (b) from irradiated surface

As shown in Fig. 8, the irradiation-induced hardening of 18Cr-ODS is observed to be lower to that of the conventional 18Cr steel. This effect can be attributed to the high density of grain boundaries and the presence of dispersed ultra-fine oxide particles within the 18Cr-ODS material, which serve as effective sinks for point defects generated during irradiation. The incorporation of a substantial density of point defect recombination centers (point defect sinks) has been identified as a successful strategy in the development of radiation tolerant materials. This approach is supported by kinetic rate theory models [15, 16], which have demonstrated a significant decrease in point defect supersaturation values and associated phenomena such as void swelling and radiation-induced solute segregation when high sink strengths are present [17]. ODS-modifications that enhance sink strength also contribute to effective mitigation of low-temperature radiation-induced hardening. In this context, 18Cr-ODS might exhibit a reduced susceptibility to embrittlement caused by irradiation.

Irradiation hardening of both HEA and ODS-HEA is characterized by lower values compared to reference austenitic steels. This is attributed to the formation and evolution of irradiation-induced defect clusters and dislocation loops, which are influenced by a higher configurational entropy and a highly distorted lattice, which inherent HEA materials. These factors result in a smaller mean size and lower density of dislocation loops, leading to a decrease in radiation hardening [18]. The high configurational entropy also modifies the point defect recombination processes, potentially resulting in radiation resistance that differs from conventional alloys [17]. Furthermore, some atomistic simulations and experimental findings suggest that the suppression of accumulated damage level in more complex and disordered alloys may be due to modified migration barriers and limited atomic diffusion [19]. The energy barrier for the movement of atom between positions with different lattice potential energies can make this process energetically unfavorable. This can decrease the overall mobility of interstitials and vacancies, hinder the formation and growth of defect clusters and dislocation loops, and promote the recombination of vacancy-interstitial pairs, which affects the overall irradiation response of these materials. Meanwhile, the irradiation hardening of the ODS-HEA is approximately the same as that of ordinary HEA, and additional studies are required to interpret such behavior.

The irradiation hardening degree of T91-MSPD and T91-M is nearly equivalent when the irradiation dose is approximately 10 dpa. Although the initial strength and density of sinks are different in T91-M and T91-MSPD steels, it appears that the formation of defect clusters and Ar-associated nano-bubbles in a similar manner influences the hardening behavior of steels under argon-ion irradiation.

Overall, the magnitude of hardening of the Ti-MPEA and T91-modified BCC-structured alloys studied here is nearly half that of the austenitic reference steels, indicating a lower susceptibility to embrittlement.

BCC metals are generally considered to have superior radiation tolerance compared to FCC metals. This belief is largely based on extensive research demonstrating that ferritic steels, which have a BCC structure, show significantly less void swelling than their austenitic (FCC) counterparts under identical irradiation conditions [20].

Research suggests that BCC metals surpass FCC metals in terms of primary defect production and defect evolution behavior [21–23]. BCC metals not only exhibit lower overall fractions of large defect clusters but also a more finely dispersed distribution of these clusters within energetic displacement cascades. This

fine dispersion of primary defects can lead to more efficient defect recombination during subsequent microstructural evolution, thereby enhancing the radiation resistance of BCC metals.

Despite the observed superior radiation resistance of BCC materials, the underlying physical mechanisms are not fully understood. Potential contributing factors include reduced in-cascade production of sessile point defect clusters, lower dislocation bias, and higher self-diffusion coefficients. The latter, in particular, is known to be generally higher in BCC metals at a given homologous temperature, which enhances self-recovery diffusion mechanisms and suppresses radiation damage accumulation [17].

Combining a radiation-resistant BCC matrix with the high sink density provided by nanoscale dispersoids has the potential to advance the creation of radiation-resistant materials with superior performance characteristics. An example of this approach could be the modification of BCC-based multi- principal element alloys using oxide dispersion strengthening techniques.

CONCLUSIONS

A series of new alloys with FCC and BCC phase structures were used to measure the effect of ion irradiation on hardening after exposure to 1.4 MeV Ar ions at room temperature. The study examined the nanohardness of these materials in the initial state, the dependence of hardening parameters on irradiation dose, and the relationship of these parameters with microstructure evolution. The obtained data was compared to that of conventional stainless steels. The following conclusions were drawn:

Irradiation hardening is associated with dislocation loops and radiation-induced Ar-filled cavity formation.

All new alloys exhibited a reduced susceptibility to irradiation induced hardening compared to that of conventional SS316 and 18Cr10NiTi stainless steels.

Modification of conventional 18Cr steel with ODS increases its sink strength for radiation defects, mitigating low-temperature radiation-induced hardening and reducing its susceptibility to irradiation-induced embrittlement.

HEA materials showed reduced irradiation hardening due to their unique properties, associated with high configurational entropy and sluggish diffusion.

BCC-structured alloys exhibit approximately 50% less irradiation hardening than austenitic reference steels, suggesting a lower susceptibility to embrittlement due to more efficient defect recombination and higher self-diffusion coefficients.

ACKNOWLEDGEMENTS

This work was financially supported by the National Academy of Science of Ukraine (program “Fundamental scientific research on the most important problems of the development of scientific and technical, socio-economic, socio-political, human potential to ensure Ukraine's competitiveness in the world and sustainable development of society and the state”).

REFERENCES

1. V.N. Voyevodin, G.D. Tolstolutskaya, M.A. Tikhonovsky, A.S. Kuprin, A.S. Kalchenko. Mechanisms of radiation damage and development of structural materials for operating and advanced nuclear reactors // *PAST*. 2021, N 5(135), p. 3-20.

2. F. Bergner, F. Gillemot, M. Hernández-Mayoral, M. Serrano, G. Török, A. Ulbricht, E. Altstadt. Contributions of Cu-rich clusters, dislocation loops and nanovoids to the irradiation-induced hardening of Cu-bearing low-Ni reactor pressure vessel steels // *J. Nucl. Mater*. 2015, v. 461, p. 37-44.

3. G.R. Odette, T. Yamamoto, T.J. Williams, R.K. Nanstad, C.A. English. On the history and status of reactor pressure vessel steel ductile to brittle transition temperature shift prediction models // *J. Nucl. Mater*. 2019, v. 526, p. 151863.

4. O.M. Velikodnyi, R.V. Vasilenko, O.S. Kalchenko, I.V. Kolodyi, E.O. Krainyuk, A.V. Levenets, P.I. Stoev, M.A. Tikhonovsky, G.D. Tolstolutska. Structure and mechanical properties of Ti-Cr-Al-Nb and Ti-Cr-Al-Nb-V multicomponent alloys // *PAST*. 2023, N 5(147), p. 59-67.

5. G. Tolstolutska, M. Tikhonovsky, O. Velikodnyi, S. Karpov, V. Ruzhytskyi, G. Tolmachova, R. Vasilenko. Hardening of lightweight multi-principal element titanium-based alloy under Ar ion irradiation // *PAST*. 2023, N 5(147), p. 3-8.

6. V.N. Voyevodin, S.A. Karpov, G.D. Tolstolutskaya, M.A. Tikhonovsky, A.N. Velikodnyi, I.E. Kopanets, G.N. Tolmachova, A.S. Kalchenko, R.L. Vasilenko, I.V. Kolodiy. Effect of irradiation on microstructure and hardening of Cr–Fe–Ni–Mn high-entropy alloy and its strengthened version // *Phil. Mag.* 2020, v. 100, N 7, p. 822-836.

7. A.N. Velikodnyi, V.N. Voyevodin, A.S. Kalchenko, S.A. Karpov, I.V. Kolodiy, M.A. Tikhonovsky, G.D. Tolstolutskaya, F.A. Garner. Impact of nano-oxides and injected gas on swelling and hardening of 18Cr10NiTi stainless steel during ion irradiation // *J. Nucl. Mater*. 2022, v. 565, p. 153666.

8. V.N. Voyevodin, G.D. Tolstolutskaya, S.A. Karpov, A.N. Velikodnyi, M.A. Tikhonovsky, A.S. Kalchenko, G.N. Tolmachova, R.L. Vasilenko, I.E. Kopanets. Effect of severe plastic deformation on radiation hardening of T91 ferritic-martensitic steel // *PAST*. 2021, N 2(132), p. 35-42.

9. G.D. Tolstolutskaya, V.V. Ruzhytskiy, S.A. Karpov, I.E. Kopanets. Retention and features of deuterium detrapping from radiation-induced damages in steels // *PAST*. 2009, N 4(62), p. 29-41.

10. S.A. Karpov, G.D. Tolstolutskaya, B.S. Sungurov, A.Y. Rostova, G.N. Tolmacheva, I.E. Kopanets. Hardening of SS316 stainless steel caused by the irradiation with argon ions // *Materials Science*. 2016, v. 52 (3), p. 377-384.

11. Pedro E.J. Rivera-Díaz-del-Castilloa and Hanwei Fu. Strengthening mechanisms in high-entropy alloys: Perspectives for alloy design // *J. Mater. Res*. 2018, v. 33, N 19, p. 2970-2982.

12. Liyuan Liu, Yang Zhang, Jihong Han, Xiyu Wang, Wenqing Jiang, Chain-Tsuan Liu, Zhongwu Zhang, and Peter K. Liaw. Nanoprecipitate-Strengthened High-Entropy Alloys // *Advanced Science*. 2021, v. 8, p. 2100870.

13. G.S. Was et al. Emulation of neutron irradiation effects with protons: validation of principle // *J. Nucl. Mater.* 2002, v. 300, p. 198-216.

14. M. Klimiankou, R. Lindau, A. Möslang. Energy-filtered TEM imaging and EELS study of ODS particles and argon-filled cavities in ferritic-martensitic steels // *Micron.* 2005, v. 36, p. 1-8.

15. L.K. Mansur. Theory and experimental background on dimensional changes in irradiated alloys // *J. Nucl. Mater*. 1994, v. 216, p. 97-123.

16. A.D. Brailsford, R. Bullough. The rate theory of swelling due to void growth in irradiated metals // *J. Nucl. Mater.* 1972, v.44, p. 121-135.

17. S.J. Zinkle and L.L. Snead. Designing Radiation Resistance in Materials for Fusion Energy *// Annu. Rev. Mater. Res.* 2014, v. 44, p.241-267.

18. W.-Y. Chen, X. Liu and Y. Chen. Irradiation effects in high entropy alloys and 316H stainless steel at 300°C // *J. Nucl. Mater*. 2018, v. 510, p. 421-430.

19. M.W. Ullah, D.S. Aidhy, Y. Zhang, W.J. Weber. Damage accumulation in ion-irradiated Ni-based concentrated solid-solution alloys // *Acta Mater.* 2016, v. 109, p. 17-22.

20. E.A. Little, R. Bullough, M.H. Wood. On the swelling resistance of ferritic steel // *Proc. R. Soc. Lond. A Math. Phys. Sci*. 1997, v. 372, p. 565-579.

21. R.C. Pasianot, A.M. Monti, G. Simonelli, E.J. Savino. Computer simulation of SIA migration in bcc and hcp metals // *J. Nucl. Mater.* 2000, v. 276, p. 230-234.

22. N. Hashimoto, S. Sakuraya, J. Tanimoto, S. Ohnuki. Effect of impurities on vacancy migration energy in Fe-based alloys // *J. Nucl. Mater.* 2014, v. 445, p. 224-226.

23. C.H. Woo, B.N. Singh. Production bias due to clustering of point defects in irradiation-induced cascades // *Phil. Mag*. A 1992, v. 65, p. 889-912.

Article received 04.04.2024

ЗМІЦНЕННЯ СУЧАСНИХ КОНСТРУКЦІЙНИХ СПЛАВІВ ПІД ВПЛИВОМ ІОННОГО ОПРОМІНЕННЯ

Г.Д. Толстолуцька, М.А. Тихоновський, С.О. Карпов, В.К. Карпач

Низка нещодавно розроблених сплавів, включаючи багатокомпонентні сплави з ОЦК- і ГЦК-структурою, аустенітну сталь, модифіковану ДЗО, і феритомартенситну сталь Т91, модифіковану інтенсивною пластичною деформацією, була досліджена з точки зору явища зміцнення/крихкості під впливом опромінення. Зразки всіх матеріалів опромінювали за однакових умов іонами Ar з енергією 1,4 МеВ при кімнатній температурі. Для характеристики радіаційних дефектів і мікроструктурних змін використовували трансмісійну електронну мікроскопію (ТЕМ). Для вимірювання впливу іонного опромінення на зміцнення використовували метод наноіндентування. Досліджено залежність параметрів зміцнення від дози опромінення, їх зв'язок з еволюцією мікроструктури. Встановлено, що розроблені сплави демонструють знижену сприйнятливість до радіаційно-індукованого зміцнення в порівнянні з традиційними нержавіючими сталями SS316 та 18Cr10NiTi. Обговорюються механізми, які можуть впливати на радіаційне зміцнення досліджуваних матеріалів.